

Nonparametric identification of structural modifications in Laplace domain

G. Suwała and L. Jankowski*

*Institute of Fundamental Technological Research (IPPT PAN), Polish Academy of Sciences,
ul. Pawińskiego 5B, 02-106 Warsaw, Poland*

Abstract

This paper proposes and experimentally verifies a Laplace-domain method for identification of structural modifications, which (1) unlike time-domain formulations, allows the identification to be focused on these parts of the frequency spectrum that have a high signal-to-noise ratio, and (2) unlike frequency-domain formulations, decreases the influence of numerical artifacts related to the particular choice of the FFT exponential window decay. In comparison to the time-domain approach proposed earlier, advantages of the proposed method are smaller computational cost and higher accuracy, which leads to reliable performance in more difficult identification cases. Analytical formulas for the first- and second-order sensitivity analysis are derived. The approach is based on a reduced nonparametric model, which has the form of a set of selected structural impulse responses. Such a model can be collected purely experimentally, which obviates the need for design and laborious updating of a parametric model, such as a finite element model. The approach is verified experimentally using a 26-node lab 3D truss structure and 30 identification cases of a single mass modification or two concurrent mass modifications.

Keywords: Structural health monitoring (SHM), Nonparametric model, Inverse problem, Virtual distortion method (VDM), Structural reanalysis, Sensitivity analysis, Laplace domain

1. Introduction

Structural health monitoring (SHM), an important field of research at the crossroads of structural engineering and signal processing, has undergone a rapid development in the last two decades [1, 2]. A typical SHM system combines a sensor network, a data transmission and processing subsystem and a central unit, which interact in collecting and analyzing measurement data in order to detect, localize and quantify structural damages, modifications or loads [3, 4]. Such systems are applied mainly in civil engineering [5, 6] and in aerospace industry [7].

In general, all existing SHM methods can be classified into two fundamental groups of local and global approaches. Local approaches, which have evolved from nondestructive testing (NDT), are used for detection and assessment of small defects in relatively narrow inspection zones via techniques that range from eddy currents [8] or thermography [9] to guided ultrasonic waves [10, 11]. Global approaches analyze changes in global low-frequency structural response and relate them to structural damages or loads. They aim at identification of globally significant factors in a large inspection zone, which is usually the entire monitored structure. Compared to local methods, their important advantage lies in the ability to identify modifications relatively distant from the sensors, so that a sparse sensor network can be used to monitor a large and complex structure. On the other hand, global methods are relatively insensitive to damages at their onset, which is related to the low sensitivity of global structural characteristics to small local structural modifications.

Most of the global SHM methods can be further classified [12, 13] as (1) parametric/model-based or (2) nonparametric/data-driven. Parametric methods rely on a parametric numerical model of the monitored

*Corresponding author. Tel.: +48 221 8261281 ext. 428. Email: ljank@ippt.pan.pl

structure, where a finite element model is usually used [14], but for simpler structures a continuous model might be also appropriate [15]. Identification amounts to minimization of an objective function, which is a certain measure of discrepancy between the experimentally measured and numerically modeled structural responses [16]. Minimization is performed with respect to selected model parameters, which are assumed to represent unknown structural modification. Model-based methods are thus deeply rooted in model-updating methods [17] and in general capable of full identification of damages [18] (detection, localization and quantification). An important appealing factor, the physical meaningfulness of structural models and identified damages, constitutes also an important weakness of parametric methods: designing and updating a reliable parametric model of a structure is often a challenging problem [19].

Nonparametric or data-driven methods obviate the need for parametric structural models [20] at the cost of their flexible physicality. Such methods rely on a database of numerical fingerprints, which are directly extracted from experimentally measured structural responses. The fingerprints are often modal [21, 22] or based on wavelet [23, 24] or time series analysis [25, 26]; they play the role of a nonparametric model of the unmodified structure. Damage is detected by recognizing a significant discrepancy between the database and the fingerprints extracted from the recent measurements; limited localization is possible by a proper distribution of sensors and local comparison of the fingerprints [27]. Further improvement in localization and quantification of structural modifications is possible only if fingerprints representing various modification scenarios are included in the database: pattern recognition procedures can be then applied to identify the best-fitting scenario [28, 29]. Such an approach is problematic with real-world civil structures, where it is rarely possible to actually introduce the damages, much less in a large number of scenarios.

This paper aims at bridging the gap between parametric and data-driven approaches, which is a goal shared with certain techniques that involve experimental and operational modal analysis [30]. On one hand, the method proposed here uses a reduced nonparametric model of the unmodified structure, which consists of its selected impulse response functions and can be collected purely experimentally: no time-consuming and error-prone model updating is thus required. On the other hand, although nonparametric, such a model allows parametrically defined modifications to be modeled, quantified and identified. Unlike the time-domain approach investigated earlier in [31], the method proceeds in Laplace domain, which decreases the computational costs by two to three orders of magnitude and significantly improves the accuracy by focusing the identification on high signal-to-noise parts of the entire frequency spectrum. Moreover, unlike frequency-domain analysis, the Laplace-domain computations average out numerical artifacts related to the particular choice of the decay rate of the FFT exponential window.

The paper is structured as follows: the next section first discusses the direct problem in the time-domain setting, and then proposes a Laplace-domain formulation. Section 3 defines the inverse problem and derives analytical formulas for the first- and second-order sensitivity analysis. Section 4 uses the mass identification problem proposed earlier in [31] for experimental verification, comparison and discussion of the obtained results. Section 5 concludes the paper.

2. The direct problem

This section starts with a summary of the time-domain approach [31], and extends it to include stiffness modifications in addition to mass modifications. Then, its shortcomings are discussed and a solution in Laplace domain is proposed.

The direct problem is understood as the problem of computing the response \mathbf{u} of the modified structure (which is stated in time domain as $\mathbf{u}(t)$, in frequency domain as $\mathbf{u}(\omega)$ or in Laplace domain as $\mathbf{u}(s)$) to a known testing excitation \mathbf{f} , given the structural modifications and certain nonparametric characteristics of the unmodified structure. The unmodified structure is assumed to be linear, and its modifications are expressed in terms of the modifications $\Delta\mathbf{M}$ and $\Delta\mathbf{K}$ of the structural mass and stiffness matrices \mathbf{M} and \mathbf{K} . The required structural characteristics are purely experimental in nature and consist of

1. the response \mathbf{u}^L of the unmodified structure to the same testing excitation \mathbf{f} , and
2. the matrix \mathbf{B} of impulse responses of the unmodified structure, which are applied/measured in the degrees of freedom (DOFs) related to the testing excitation, potential modifications and sensors.

The matrix \mathbf{B} constitutes in fact a nonparametric model of the unmodified structure, which is reduced with respect to the DOFs involved in the testing excitation, measurements and modifications.

The formulation is based on the virtual distortion method (VDM) [32], which is a flexible method for quick reanalysis that has been used for modeling and identification of structural modifications of various nature [33], including material damping [34], plastic strains [35], virtual supports [36], etc. The effects of the modifications are modeled with a vector \mathbf{p} of the equivalent pseudo loads that act in the unmodified structure. The response \mathbf{u} of the *modified structure* to the excitation \mathbf{f} is expressed as a sum of

1. the response \mathbf{u}^L of the *unmodified structure* to \mathbf{f} , and
2. the cumulative effect \mathbf{u}^R of the pseudo loads on the response, which is expressed in the form of their convolution Eq. (2) with the impulse responses included in the matrix \mathbf{B} .

The response of the modified structure is found in two steps: first the pseudo loads are computed and then the corresponding response. The pseudo loads are coupled to the response, hence they are given in the implicit form of a certain integral equation, whose solution in time domain is computationally a very demanding task, which is one of the shortcomings of the time-domain approach proposed in [31].

2.1. Time-domain formulation

Let $\mathbf{p}(t)$ be a vector of (arbitrary) pseudo loads that excite the original unmodified structure. Denote by $\mathbf{u}^R(t)$ the vector of the corresponding structural response. The unmodified structure is assumed to satisfy the equation of motion,

$$\mathbf{p}(t) = \mathbf{M}\ddot{\mathbf{u}}^R(t) + \mathbf{C}\dot{\mathbf{u}}^R(t) + \mathbf{K}\mathbf{u}^R(t), \quad (1)$$

where \mathbf{M} , \mathbf{C} and \mathbf{K} denote respectively the mass, damping and stiffness matrices. Since the structure is linear, assuming zero initial conditions, its response can be expressed in the form of a convolution of the excitation $\mathbf{p}(t)$ with the matrix $\mathbf{B}(t)$ of structural impulse responses,

$$\mathbf{u}^R(t) = \int_0^t \mathbf{B}(t-\tau)\mathbf{p}(\tau) d\tau, \quad (2a)$$

$$\ddot{\mathbf{u}}^R(t) = \int_0^t \ddot{\mathbf{B}}(t-\tau)\mathbf{p}(\tau) d\tau. \quad (2b)$$

Let $\mathbf{f}(t)$ be an external testing excitation, and denote respectively by $\mathbf{u}^L(t)$ and $\mathbf{u}(t)$ the responses of the unmodified and modified structures. If the effect of the modifications on structural damping is neglected, the corresponding equations of motion can be stated as

$$\mathbf{f}(t) = \mathbf{M}\ddot{\mathbf{u}}^L(t) + \mathbf{C}\dot{\mathbf{u}}^L(t) + \mathbf{K}\mathbf{u}^L(t), \quad (3)$$

$$\mathbf{f}(t) = (\mathbf{M} + \Delta\mathbf{M})\ddot{\mathbf{u}}(t) + \mathbf{C}\dot{\mathbf{u}}(t) + (\mathbf{K} + \Delta\mathbf{K})\mathbf{u}(t), \quad (4)$$

where $\Delta\mathbf{M}$ and $\Delta\mathbf{K}$ model the modifications. Equation (4) can be rearranged into the equation of motion of the unmodified structure,

$$\mathbf{f}(t) + \mathbf{p}(t) = \mathbf{M}\ddot{\mathbf{u}}(t) + \mathbf{C}\dot{\mathbf{u}}(t) + \mathbf{K}\mathbf{u}(t), \quad (5)$$

where the modifications are modeled by the pseudo load $\mathbf{p}(t)$,

$$\mathbf{p}(t) = -\Delta\mathbf{M}\ddot{\mathbf{u}}(t) - \Delta\mathbf{K}\mathbf{u}(t). \quad (6)$$

The unmodified structure is linear, thus as seen in Eq. (5), the response $\mathbf{u}(t)$ is the sum of the responses of the unmodified structure to $\mathbf{f}(t)$ and $\mathbf{p}(t)$, which are respectively $\mathbf{u}^L(t)$ and $\mathbf{u}^R(t)$, see Eqs. (3) and (1),

$$\mathbf{u}(t) = \mathbf{u}^L(t) + \mathbf{u}^R(t). \quad (7)$$

If Eq. (7) is substituted into Eq. (6) and then Eqs. (2) are used, the following equation is obtained:

$$-\Delta\mathbf{M}\ddot{\mathbf{u}}^L(t) - \Delta\mathbf{K}\mathbf{u}^L(t) = \mathbf{p}(t) + \Delta\mathbf{M} \int_0^t \ddot{\mathbf{B}}(t-\tau)\mathbf{p}(\tau) d\tau + \Delta\mathbf{K} \int_0^t \mathbf{B}(t-\tau)\mathbf{p}(\tau) d\tau, \quad (8)$$

which is a system of Volterra integral equations with the pseudo load vector $\mathbf{p}(t)$ as the unknown. Even if ill-conditioned, Eq. (8) is well-posed, provided $\mathbf{M} + \Delta\mathbf{M}$ is non-singular [31]. Therefore, Eq. (8) has a unique solution, if the mass modification upholds the positive definiteness of the mass matrix $\mathbf{M} + \Delta\mathbf{M}$.

For a given testing excitation $\mathbf{f}(t)$, the pseudo load equivalent to given modifications $\Delta\mathbf{M}$ and $\Delta\mathbf{K}$ is found by solving Eq. (8). According to Eqs. (7) and (2), the response of the modified structure is the following sum of the response of the unmodified structure and the cumulative effect of the pseudo load:

$$\mathbf{u}(t) = \mathbf{u}^L(t) + \int_0^t \mathbf{B}(t - \tau)\mathbf{p}(\tau) d\tau, \quad (9a)$$

$$\ddot{\mathbf{u}}(t) = \ddot{\mathbf{u}}^L(t) + \int_0^t \ddot{\mathbf{B}}(t - \tau)\mathbf{p}(\tau) d\tau. \quad (9b)$$

Besides $\Delta\mathbf{M}$ and $\Delta\mathbf{K}$, the computations require only a reduced nonparametric model of the unmodified structure, which consists of its selected characteristics that can be measured experimentally:

1. the responses $\mathbf{u}^L(t)$ and/or $\ddot{\mathbf{u}}^L(t)$ to the excitation $\mathbf{f}(t)$,
2. the impulse response matrices $\mathbf{B}(t)$ and/or $\ddot{\mathbf{B}}(t)$.

As a result, there is no need to build and update a complete parametric model of neither the unmodified nor the modified structure. According to Eq. (6), the pseudo loads are nonzero only in the DOFs related to the modifications, which allows the number of necessary measurements to be significantly restricted.

2.2. Discussion and Laplace-domain solution

The crucial step in the time-domain approach is the solution of Eq. (8), which after time discretization constitutes a large, dense and extremely ill-conditioned system of linear equations with a block-Toeplitz structure. In [31], several efficient numerical techniques have been exploited, including block embedment in larger circulant matrices, computing exact matrix-vector products by the fast Fourier transform (FFT) and a regularizing iterative solution scheme through the conjugate gradient least squares (CGLS) algorithm. However, even with these techniques, the time-domain computations are numerically very expensive, while the results remain sensitive to parameters such as the number of time steps used in computations.

The technique proposed in this paper uses the Laplace transform; the derivation parallels Eqs. (1) to (7). The transform converts the time-domain Eq. (8) into the following small Laplace-domain system:

$$-\Delta\mathbf{M}\ddot{\mathbf{u}}^L(s) - \Delta\mathbf{K}\mathbf{u}^L(s) = \left[\mathbf{I} + \Delta\mathbf{M}\ddot{\mathbf{B}}(s) + \Delta\mathbf{K}\mathbf{B}(s) \right] \mathbf{p}(s), \quad (10)$$

where

$$s = \eta + i\omega \in \mathbb{C} \quad (11)$$

and $\mathbf{B}(s)$ and $\ddot{\mathbf{B}}(s)$ are the Laplace-domain counterparts of the impulse response matrices $\mathbf{B}(t)$ and $\ddot{\mathbf{B}}(t)$. Solved Eq. (10), the response of the modified structure is obtained by the counterparts of Eqs. (9),

$$\mathbf{u}(s) = \mathbf{u}^L(s) + \mathbf{B}(s)\mathbf{p}(s), \quad (12a)$$

$$\ddot{\mathbf{u}}(s) = \ddot{\mathbf{u}}^L(s) + \ddot{\mathbf{B}}(s)\mathbf{p}(s). \quad (12b)$$

The Laplace-domain Eq. (10) constitutes an independent system for each s from the domain of convergence. It is a huge computational advantage over the time-domain approach, which computes the solution for all frequencies at once. On the other hand, a disadvantage is that the fine time-domain control over the regularization process offered by the CGLS algorithm is lost [37]. As a result, using the inverse Laplace transform to compute the time-domain responses from the Laplace-domain responses Eqs. (12) will rarely yield a numerically meaningful result. It suggests that

- The Laplace-domain response of the modified structure can be reliably computed only for a certain bounded subset \mathbf{L} of the theoretical half-plane of absolute convergence defined as $\text{Re } s > \eta_{\min}$. The reliability level depends on several factors:

- Numerical conditioning of Eq. (10): reliable computations are possible only if the system is not excessively ill-conditioned.
 - Reliability of the nonparametric structural model at the considered frequency line $\omega = \text{Im } s$: meaningful computations are possible only if ω is well-represented in the experimental quasi-impulsive excitations used to generate the impulse response matrices $\mathbf{B}(t)$ and $\ddot{\mathbf{B}}(t)$.
 - Measurement time interval: in practice, measurement time interval is finite, and in order to avoid spectral leakage, the decay rate η should be positive and high enough to ensure proper attenuation of the measured signals at the end of the interval.
 - Measurement sampling rate: in practice, measurement signal is discrete, and the usable range of $\omega = \text{Im } s$ is limited by the sampling frequency.
- The inverse problem of identification should be based on the Laplace-domain representation of the structural response (in its domain of reliability) instead of the time-domain histories.

3. Inverse problem

The inverse problem is the problem of identification of the unknown structural modifications $\Delta\mathbf{M}$ and $\Delta\mathbf{K}$, based on the

1. measured response of the modified structure \mathbf{u}^{M} to the testing excitation \mathbf{f} ,
2. measured reference response of the unmodified structure \mathbf{u}^{L} to the same testing excitation \mathbf{f} , and
3. nonparametric model of the unmodified structure, given in the form of the matrices \mathbf{B} and $\ddot{\mathbf{B}}$ of the experimentally measured structural impulse responses.

A significant discrepancy between the measured response \mathbf{u}^{M} and the reference response \mathbf{u}^{L} suggests that a modification has occurred. The modification can be then identified by minimizing the discrepancy between the measured response and the response modeled nonparametrically in the direct problem.

It is assumed that the unknown structural modifications are defined in terms of the vector

$$\boldsymbol{\mu} = [\mu_1, \mu_2, \dots, \mu_N]^{\text{T}} \quad (13)$$

of certain modification parameters, which can affect only mass (added masses), only stiffness (Young moduli) or both (element cross-sections). As a result, identification of the modifications $\Delta\mathbf{M}(\boldsymbol{\mu})$ and $\Delta\mathbf{K}(\boldsymbol{\mu})$ amounts to the identification of the equivalent vector $\boldsymbol{\mu}$ of modification parameters.

3.1. Objective function

The vague notion of discrepancy is formalized in the form of the following objective function:

$$F(\boldsymbol{\mu}; \mathbf{f}) := \frac{1}{2} \langle \mathbf{d}, \mathbf{d} \rangle, \quad (14)$$

where $\boldsymbol{\mu}$ is the unknown vector of modification parameters that needs to be identified, \mathbf{f} is the testing excitation, and $\mathbf{d}(s)$ is the Laplace-domain difference between the measured response $\mathbf{u}^{\text{M}}(s)$ and the non-parametrically modeled response $\mathbf{u}(s)$,

$$\mathbf{d}(s) := \mathbf{u}^{\text{M}}(s) - \mathbf{u}(s). \quad (15)$$

The scalar product $\langle \cdot, \cdot \rangle$ is defined as

$$\langle \mathbf{g}, \mathbf{h} \rangle := \iint_{\mathbf{L}} \mathbf{h}^{\text{H}}(s) \mathbf{g}(s) d\eta d\omega, \quad (16)$$

where η and ω are respectively the real and imaginary parts of s , see Eq. (11), the upper index H denotes the conjugate transpose, and $\mathbf{L} \subset \mathbb{C}$ is the assumed domain of reliability, which can be determined based

on the reliability criteria outlined in Section 2.2. In practice, to facilitate a comparison between objective functions computed in different identification cases, it might be useful to normalize Eq. (14) with respect to the measured response by dividing F by $\langle \mathbf{u}^M, \mathbf{u}^M \rangle$.

The identification process is equivalent to minimization of the objective function Eq. (14). In the following, a fast method is proposed to compute its first and second derivatives, which allows classical Newton or quasi-Newton optimization algorithms to be used for quick local convergence. The initial optimization point can be selected arbitrarily or using heuristic randomization approaches to avoid local minima.

3.2. First-order sensitivity analysis

Direct differentiation of the objective function Eq. (14) with respect to the modification parameter μ_i yields

$$F_i(\boldsymbol{\mu}; \mathbf{f}) := \frac{\partial}{\partial \mu_i} F(\boldsymbol{\mu}; \mathbf{f}) = -\langle \mathbf{d}, \mathbf{u}_i \rangle, \quad (17)$$

where $\mathbf{u}_i(s)$ is the corresponding derivative of the response $\mathbf{u}(s)$ that, by a direct differentiation of Eq. (12a), can be expressed in terms of the derivative $\mathbf{p}_i(s)$ of the pseudo load,

$$\mathbf{u}_i(s) := \frac{\partial}{\partial \mu_i} \mathbf{u}(s) = \mathbf{B}(s) \mathbf{p}_i(s). \quad (18)$$

The direct differentiation method (DDM) of sensitivity analysis [38] computes the derivatives of the pseudo loads by solving the respectively differentiated Eq. (10),

$$-\Delta \mathbf{M}_i \ddot{\mathbf{u}}(s) - \Delta \mathbf{K}_i \mathbf{u}(s) = \left[\mathbf{I} + \Delta \mathbf{M} \ddot{\mathbf{B}}(s) + \Delta \mathbf{K} \mathbf{B}(s) \right] \mathbf{p}_i(s), \quad (19)$$

where Eqs. (12) are used and which needs to be solved anew for each modification parameter μ_i . Solved Eq. (19), the resulting $\mathbf{p}_i(s)$ is used in Eq. (18) to compute $\mathbf{u}_i(s)$, which is then substituted into Eq. (17) to obtain $F_i(\boldsymbol{\mu}; \mathbf{f})$.

In contrast to the DDM, the adjoint variable method (AVM) [39] does not require repetitive solutions of Eq. (19). The AVM collects all the terms in Eq. (19) on the right-hand side and takes then the scalar product Eq. (16) of the result with a vector $\boldsymbol{\lambda}(s)$ of adjoint variables,

$$\begin{aligned} 0 &= \langle \boldsymbol{\lambda}, \mathbf{0} \rangle \\ &= \left\langle \boldsymbol{\lambda}, \left[\mathbf{I} + \Delta \mathbf{M} \ddot{\mathbf{B}} + \Delta \mathbf{K} \mathbf{B} \right] \mathbf{p}_i + \Delta \mathbf{M}_i \ddot{\mathbf{u}} + \Delta \mathbf{K}_i \mathbf{u} \right\rangle. \end{aligned} \quad (20)$$

The result vanishes, and it is thus added to Eq. (17). The terms that contain the derivative $\mathbf{p}_i(s)$ of the pseudo load are then grouped together,

$$F_i(\boldsymbol{\mu}; \mathbf{f}) = \left\langle -\mathbf{B}^H \mathbf{d} + \left[\mathbf{I} + \Delta \mathbf{M} \ddot{\mathbf{B}} + \Delta \mathbf{K} \mathbf{B} \right]^H \boldsymbol{\lambda}, \mathbf{p}_i \right\rangle + \langle \boldsymbol{\lambda}, \Delta \mathbf{M}_i \ddot{\mathbf{u}} + \Delta \mathbf{K}_i \mathbf{u} \rangle. \quad (21)$$

Finally, the derivative $\mathbf{p}_i(s)$ is eliminated from Eq. (21) by choosing the vector $\boldsymbol{\lambda}(s)$ of the adjoint variables in such a way that the first scalar product in Eq. (21) vanishes as a whole. It happens, if the left multiplier in the scalar product vanishes, that is if $\boldsymbol{\lambda}(s)$ is a solution to

$$\mathbf{B}^H(s) \mathbf{d}(s) = \left[\mathbf{I} + \Delta \mathbf{M} \ddot{\mathbf{B}}(s) + \Delta \mathbf{K} \mathbf{B}(s) \right]^H \boldsymbol{\lambda}(s), \quad (22)$$

which is called the adjoint equation. The derivative of the objective function is equal then to the second term in Eq. (21),

$$F_i(\boldsymbol{\mu}; \mathbf{f}) = \langle \boldsymbol{\lambda}, \Delta \mathbf{M}_i \ddot{\mathbf{u}} + \Delta \mathbf{K}_i \mathbf{u} \rangle. \quad (23)$$

Notice that Eq. (22) and the vector $\boldsymbol{\lambda}(s)$ are independent of i , so that the AVM allows the full gradient of the objective function to be obtained at the cost of only a single solution of Eq. (22). This is a significant advantage over the DDM, which requires multiple solutions of Eq. (19).

3.3. Second-order sensitivity analysis

A fast second-order sensitivity analysis can be performed using the direct–adjoint method, which seems to be the fastest from the family of second-order adjoint methods [39]. Similarly as in the first-order analysis, double differentiation of Eq. (14) with respect to μ_i and μ_j yields

$$F_{ij}(\boldsymbol{\mu}; \mathbf{f}) := \frac{\partial^2}{\partial \mu_i \partial \mu_j} F(\boldsymbol{\mu}) = \langle \mathbf{u}_j, \mathbf{u}_i \rangle - \langle \mathbf{d}, \mathbf{u}_{ij} \rangle, \quad (24)$$

where

$$\mathbf{u}_{ij}(s) := \frac{\partial^2}{\partial \mu_i \partial \mu_j} \mathbf{u}(s) = \mathbf{B}(s) \mathbf{p}_{ij}(s). \quad (25)$$

The second-order derivative $\mathbf{p}_{ij}(s)$ of the pseudo load is the solution to the double differentiated Eq. (10),

$$-\Delta \mathbf{M}_i \ddot{\mathbf{u}}_j(s) - \Delta \mathbf{M}_j \ddot{\mathbf{u}}_i(s) - \Delta \mathbf{K}_i \mathbf{u}_j(s) - \Delta \mathbf{K}_j \mathbf{u}_i(s) = \left[\mathbf{I} + \Delta \mathbf{M} \ddot{\mathbf{B}}(s) + \Delta \mathbf{K} \mathbf{B}(s) \right] \mathbf{p}_{ij}(s), \quad (26)$$

where it is assumed for notational simplicity that the modifications $\Delta \mathbf{M}$ and $\Delta \mathbf{K}$ are linear with respect to the modification parameters, that is $\Delta \mathbf{M}_{ij} = \Delta \mathbf{K}_{ij} = \mathbf{0}$.

The direct–adjoint method eliminates the direct dependence of F_{ij} on $\mathbf{p}_{ij}(s)$ by using the same procedure as in the first-order analysis: all terms in Eq. (26) are collected on the right-hand side, a scalar product is taken with the vector $\boldsymbol{\lambda}(s)$, the result is then added to Eq. (24), and the terms that contain $\mathbf{p}_{ij}(s)$ are grouped together and eliminated. As a result, the procedure yields

$$F_{ij}(\boldsymbol{\mu}; \mathbf{f}) = \langle \mathbf{u}_j, \mathbf{u}_i \rangle + \langle \boldsymbol{\lambda}, \Delta \mathbf{M}_i \ddot{\mathbf{u}}_j + \Delta \mathbf{M}_j \ddot{\mathbf{u}}_i + \Delta \mathbf{K}_i \mathbf{u}_j + \Delta \mathbf{K}_j \mathbf{u}_i \rangle, \quad (27)$$

where $\boldsymbol{\lambda}(s)$ is the solution to Eq. (22) and the derivatives $\mathbf{u}_i(s)$, $\mathbf{u}_j(s)$, $\ddot{\mathbf{u}}_i(s)$ and $\ddot{\mathbf{u}}_j(s)$ of the responses have to be computed using the first-order DDM method, that is by a repeated solution of Eq. (19). The total cost of the second-order analysis is thus linear with respect to the number of modification parameters.

4. Experimental verification

To facilitate a comparison with the results obtained earlier in [31] using the time-domain approach, this work uses the same experimental setup and the same problem of identification of added masses. However, the number of considered identification cases is enlarged and consists here of

- 12 identification cases of a single added mass (all the same as in [31]),
- 18 identification cases of two added masses (12 new cases in comparison to [31]),

The problem of identification of a single added mass is used to determine the domain \mathbf{L} of reliability, see Section 2.2. Then, the determined domain is used in the different and more complex problem of identification of two concurrent mass modifications.

4.1. Experimental setup

Structure. A 3D truss structure with 26 nodes and 70 elements is used, see Fig. 1. It is constructed using a commercial system of spherical joints and connecting tubes. The total length of the structure is 4 m; its elements are circular steel tubes with the radius of 22 mm, the wall thickness of 1 mm and the length 0.707 m (diagonal elements) or 0.500 m. The mass of each joint is 0.23 kg, and the total mass of the structure is approximately 32 kg. The two right-hand side nodes in the scheme are free to move in the longitudinal direction only, while the two opposite left-hand side nodes have all their DOFs restrained (fixed supports).

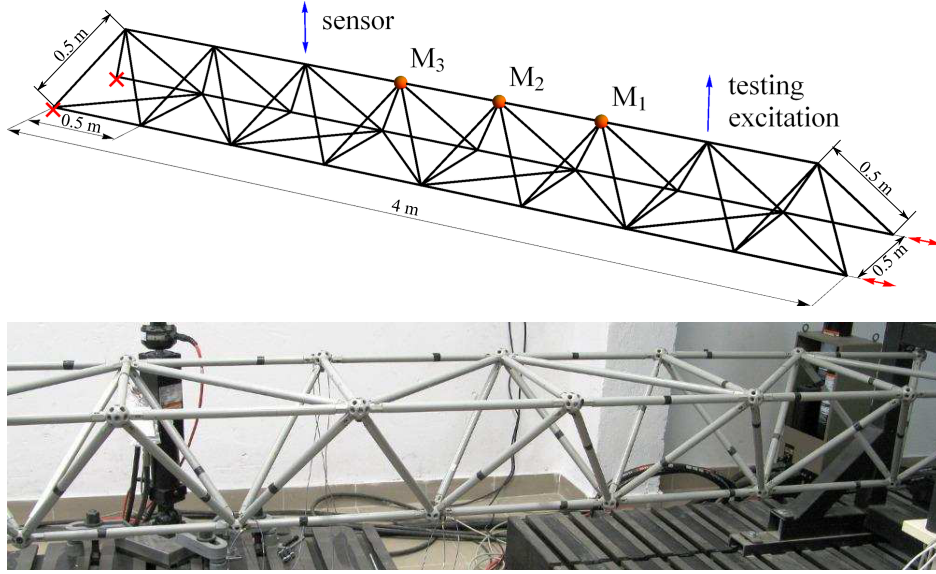


Figure 1: The 3D truss structure used for experimental verification: (top) scheme; (bottom) a fragment of the real structure

Added masses. Nodal mass modifications are implemented by attaching concentrated masses at either one or two out of the nodes marked M_1 , M_2 and M_3 in Fig. 1. A total of 30 different modifications is considered:

- *12 single nodal mass modifications:* In each of M_1 , M_2 and M_3 , the following four masses are separately attached: 1.355 kg, 2.855 kg, 3.855 kg and 5.355 kg.
- *18 modifications of two nodal masses:* In each of the three pairs of nodes, (M_1, M_3) , (M_1, M_2) and (M_2, M_3) , the following six pairs of masses are separately attached: (1.355 kg, 1.388 kg), (2.855 kg, 1.388 kg), (1.355 kg, 2.888 kg), (2.855 kg, 2.888 kg), (1.355 kg, 3.888 kg) and (2.855 kg, 3.888 kg).

Such modifications can considerably alter the local structural dynamics in their neighborhood, since they range from 100% to almost 400% of the structural mass related to the modified node (joint mass plus half of the masses of the six neighboring elements). On the other hand, in comparison to the total mass of the unmodified structure, the relative mass modifications are much smaller and range from 4.2% to 21.1%.

Instrumentation. Fig. 1(top) shows the location of the testing excitation \mathbf{f} and of the single sensor intended for identification, which is used to measure the responses \mathbf{u}^L and \mathbf{u}^M . All the involved excitations are generated using a modal hammer (Brüel & Kjær, Type 8202), while all sensors are accelerometers. The signals from the accelerometers and from the modal hammer are collected by a data acquisition system PULSE, sampled at 65.5 kHz and transferred to a desktop PC. Approximately 16 000 time steps are recorded for each response, which corresponds to the time interval of about $T = 0.240$ s or 7.7 periods of the first natural vibration (31.5 Hz). For each response, the measurements are repeated independently four times and averaged in order to decrease the influence of the measurement noise.

4.2. Discretized objective function

The integral-based definition of the objective function Eq. (14) is discretized here into a summation over a rectangular grid:

$$F(\boldsymbol{\mu}; \mathbf{f}) = \frac{1}{2} \sum_{\omega \in \mathbf{L}_\omega} \sum_{\eta \in \mathbf{L}_\eta} |\ddot{\mathbf{u}}^M(s) - \ddot{\mathbf{u}}(s)|^2, \quad (28)$$

where accelerations are used instead of the displacements because the sensors are accelerometers and the assumed domain of reliability is defined by the sets

$$\begin{aligned}\mathbf{L}_\omega &= \{\omega_1, \omega_2, \dots, \omega_{N_\omega}\}, \\ \mathbf{L}_\eta &= \{\eta_1, \eta_2, \dots, \eta_{N_\eta}\}.\end{aligned}\tag{29}$$

In order to excite several natural vibration modes of the structure, the testing excitation \mathbf{f} should have a possibly broadband character. Quasi-impulsive modal hammer excitations are thus used to compute the response to the ideal impulsive excitation in the domain of reliability \mathbf{L} . The testing excitation and the sensor used for identification are placed to capture at least the first two bending modes of the structure.

4.3. Domain of reliability

Accuracy of identification, especially in case of a high measurement noise, can strongly depend on the assumed domain of reliability and on its discretization. Here, a rectangular domain Eq. (29) is used, defined by the lower and upper bounds imposed on the frequency and the decay rate. In order to minimize the influence of the noise, the bounds have been selected based on the signal-to-noise ratio (SNR) and the identification accuracy obtained in a simple test case:

- *Spectral lines \mathbf{L}_ω .* The set \mathbf{L}_ω is determined to ensure a high SNR. The nonparametric model consists of a set of measured responses to a number of quasi-impulsive excitations q_i , which are generated in different DOFs with a modal hammer. First, the amplitudes $|q_i(\omega)|$ are computed at all frequency lines ω and for all the applied excitations indexed by i . The set \mathbf{L}_ω is then defined based on the 10% amplitude threshold level,

$$\mathbf{L}_\omega := \left\{ \omega \mid \frac{\min_i |q_i(\omega)|}{\max_{i,\omega} |q_i(\omega)|} \geq 10\% \right\},\tag{30}$$

which in terms of the excitation energy corresponds to the threshold of 1%. The criterion yields the set of the initial 94 frequency lines, which uniformly span the range from 0 Hz to 379 Hz.

- *Decay rates \mathbf{L}_η of the exponential window.* The set \mathbf{L}_η of the decay rates is determined based on the identification accuracy assessed in the simple test case of a single added mass. First, the set of all possible decay rates η is discretized using an arbitrary step of 0.1 with respect to the exponent of the attenuation rate at the end of the time window. Then, the set \mathbf{L}_η is determined by including only these values, for which the mean-square relative identification error of a single added mass does not exceed the threshold level of 3%. The criterion yields a set of 36 values, see Fig. 3 and Eq. (31).

4.4. Identification of a single added mass

The identification is performed independently in each of the 12 cases that correspond to the four masses that are successively fixed to the three considered nodes M_1 , M_2 and M_3 . It is assumed that the location of the mass is known, so that there is only a single optimization variable in each case. In order to avoid numerical instabilities, the vector of pseudo loads $\mathbf{p}(s)$ is determined by solving Eq. (10) with numerical regularization by the TSVD method at the level of 1% (truncated singular value decomposition).

Determination of the range of decay rates. In order to determine the set \mathbf{L}_η , the identification is performed separately for each considered value of the decay rate. The results are presented in Fig. 2, while their relative mean-square error is plotted in Fig. 3. The identification results depend on the decay rate, but in general they are highly accurate and stable in a wide range of the decay rates. The set \mathbf{L}_η is thus determined to consist of these of the tested values, for which the mean-square relative error remains below 3%, which yields

$$\mathbf{L}_\eta = \left\{ -\frac{1}{T} \log_{10} a \mid a \in \{1.6, 1.7, \dots, 5.1\} \right\}.\tag{31}$$

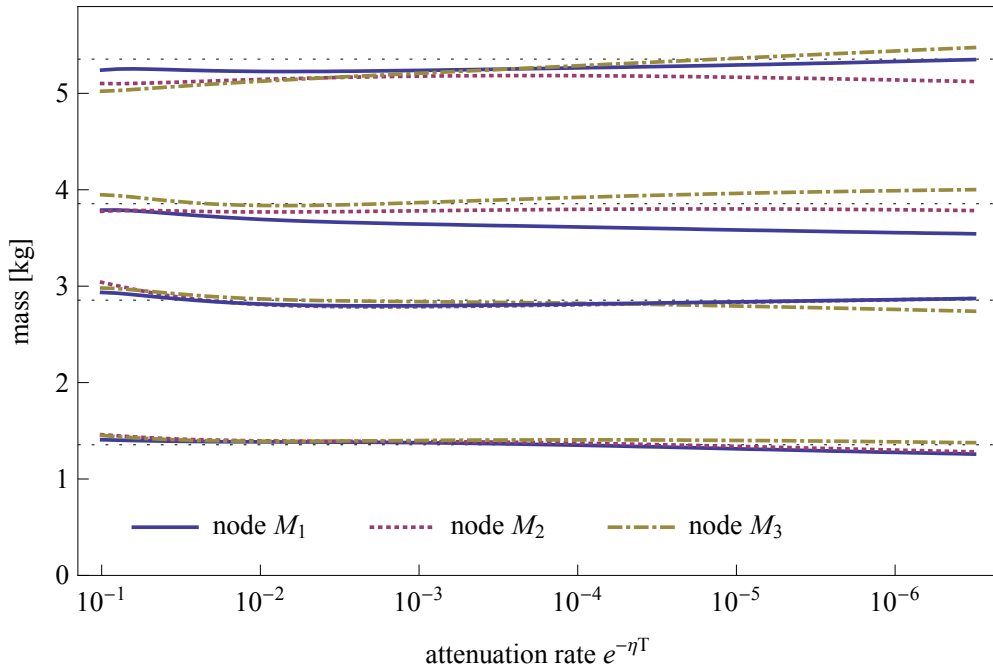


Figure 2: Identification of a single added mass in frequency domain: identified mass in dependence on the attenuation rate of the exponential FFT window at the end of the considered time interval. The actual values of added masses are marked with dotted horizontal lines

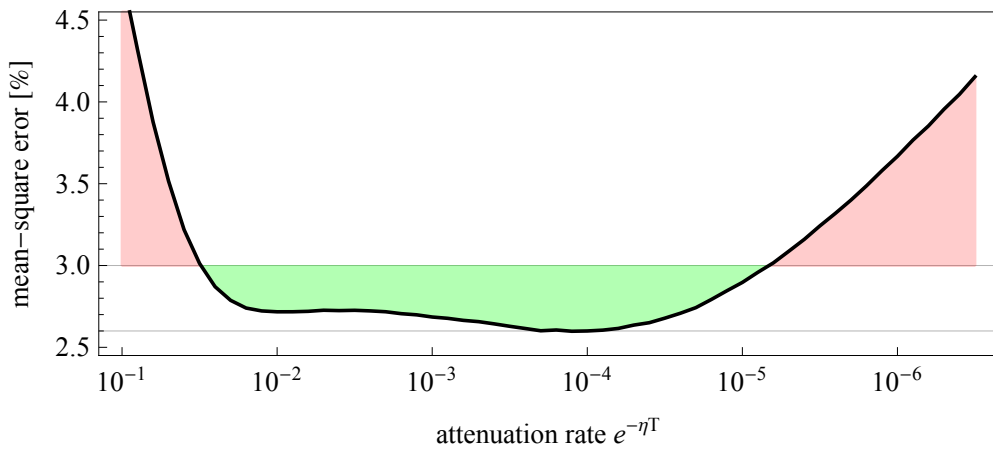


Figure 3: Identification of a single added mass in frequency domain: mean-square relative identification error in dependence on the attenuation rate of the exponential FFT window at the end of the considered time interval. The horizontal gridlines mark the assumed threshold level of 3% and the 2.6% rms error of identification in Laplace domain

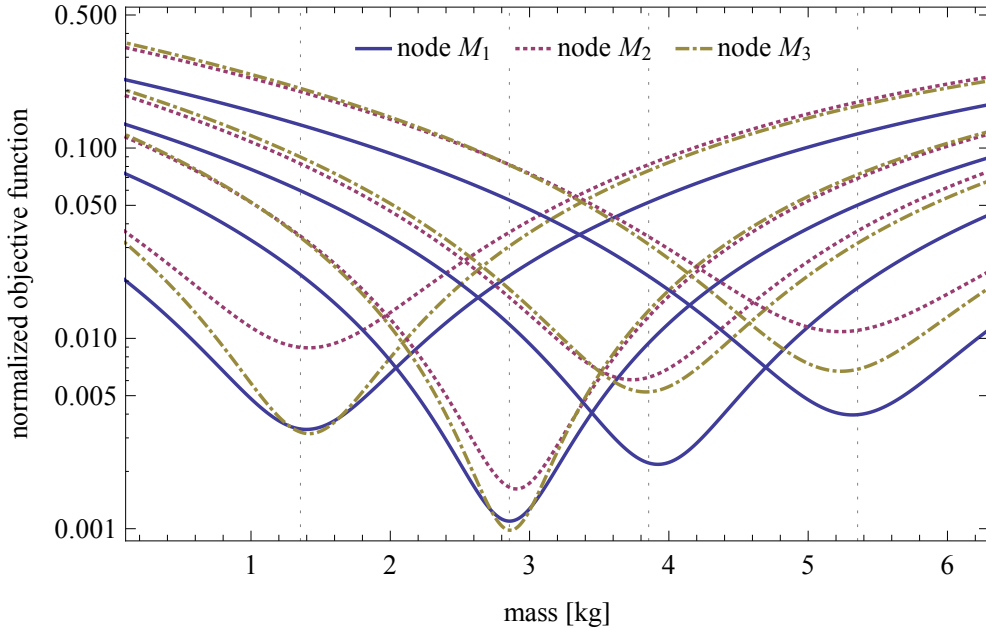


Figure 4: Identification of a single added mass in Laplace domain: normalized objective functions. The actual values of added masses are marked with dotted vertical gridlines

Laplace-domain identification. The determined domain of reliability is used for successive identification in Laplace domain, which simultaneously uses all the involved decay rates Eq. (31). Fig. 4 shows the plots of the normalized objective functions in dependence on the added mass. All objective functions are smooth and unimodal, which facilitates their numerical minimization. The values of the actually added masses are marked with dotted vertical lines. The identification results are listed in Table 1 together with their relative identification errors, which range from -4.5% to 3.1% . Statistics of the relative identification error are listed in the summary Table 3. The mean-square relative identification error equals 2.6% , which is the minimum level attained in frequency-domain identification only for specific values of the decay rate (Fig. 3) and approximately two times smaller than in the case of time-domain identification [31]. Moreover, there is no systematic underestimation of the added masses, which was apparent in the time-domain analysis.

4.5. Identification of two added masses

In the previous section, the domain of reliability is determined based on the accuracy of identification of a single added mass. In this section, the determined domain is used in the different and more complex task of identification of two concurrent mass modifications in a total of 18 cases.

For each pair of nodes separately, (M_1, M_3) , (M_1, M_2) and (M_2, M_3) , six identification cases are considered, see the second and the third column of Table 2. In each case, there are two optimization variables, m_A and m_B , which represent the masses added in the respective nodes. Identification results are listed in Table 2 and plotted in Fig. 5. Statistics of their relative accuracy are listed in Table 3. For this purpose, the relative identification errors are assessed for the total modification mass,

$$\epsilon^{\text{total}} := \frac{m_A^{\text{identified}} + m_B^{\text{identified}} - m_A^{\text{added}} - m_B^{\text{added}}}{m_A^{\text{added}} + m_B^{\text{added}}}, \quad (32)$$

as well as for each of the considered masses separately,

$$\epsilon_A := \frac{m_A^{\text{identified}} - m_A^{\text{added}}}{m_A^{\text{added}}}, \quad \epsilon_B := \frac{m_B^{\text{identified}} - m_B^{\text{added}}}{m_B^{\text{added}}}, \quad (33)$$

Table 1: Identification of a single added mass in Laplace domain: added mass, identified mass and relative identification error. The mean-square relative error equals 2.6%

Node	Added mass [kg]	Identified mass [kg]	Relative error [%]
M_1	1.355	1.376	1.6
M_1	2.855	2.813	-1.5
M_1	3.855	3.862	0.2
M_1	5.355	5.238	-2.2
M_2	1.355	1.392	2.7
M_2	2.855	2.861	0.2
M_2	3.855	3.680	-4.5
M_2	5.355	5.151	-3.8
M_3	1.355	1.397	3.1
M_3	2.855	2.818	-1.3
M_3	3.855	3.777	-2.0
M_3	5.355	5.156	-3.7

Table 2: Identification of two added masses in Laplace domain: actually added masses and identified masses for the three considered combination of nodes. Statistics of the relative identification errors are listed in Table 3.

Case No	Added masses [kg]		Identified masses [kg]					
	Nodes (A, B)		(A, B) = (M ₁ , M ₃)		(A, B) = (M ₁ , M ₂)		(A, B) = (M ₂ , M ₃)	
1	1.355	1.388	1.398	1.270	1.612	1.134	1.014	1.623
2	2.855	1.388	3.041	1.103	3.264	0.987	2.161	1.886
3	1.355	2.888	1.765	2.419	1.800	2.404	1.613	2.436
4	2.855	2.888	3.158	2.493	3.572	2.134	1.545	3.901
5	1.355	3.888	1.329	3.678	1.092	3.810	1.435	3.552
6	2.855	3.888	2.973	3.625	2.920	3.545	2.141	4.247

where the lower indices A and B denote the first and the second of the added masses, while the upper indices “identified” and “added” denote self-evidently the identified and the actually added masses.

In order to verify the robustness of the Laplace-domain approach in comparison to frequency-domain, the identification is repeated separately for each considered value of the decay rate. The relative errors of the obtained identification results are computed as in Eq. (33); their mean-square value is plotted in Fig. 6.

4.6. Discussion of results

Single added mass. In frequency domain, identification results for a single added mass are clearly dependent on the decay rate of the FFT exponential window, but still relatively stable in a wide range of decay values, see Figs. 2 and 3. The values typically used in experimental practice (1% to 4% window attenuation at the end of the considered time interval) overlap with the assumed stability range. Performing the identification in Laplace domain decreases the rms relative error to 2.6%, which is the minimum level attained in frequency domain only for specific values of the decay rate. Such a level compares very favorably to the results obtained earlier at a much larger computational cost in the time-domain analysis (5.4% for full-length responses), see Table 3. Moreover, the Laplace-domain results do not show any significant systematic underestimation of the actual values (mean relative error -0.9%), which is apparent in the time-domain analysis (mean relative error for full-length responses -5.2%).

Two added masses. The relative errors are larger in the more complex case of two concurrent mass modifications. A similar effect occurs also in time-domain analysis, and it is related to the intrinsic numerical

Table 3: Identification of added masses in Laplace and time domains: min, mean, max and rms relative errors. The time-domain results are computed for full-length responses (15 000 time steps) using the approach proposed in [31]. All results are stated in percent [%]

	Added masses identified separately				Total modification mass			
	Min	Mean	Max	Rms	Min	Mean	Max	Rms
one added mass, Laplace domain								
all cases	-4.5	-0.9	3.1	2.6	-4.5	-0.9	3.1	2.6
two added masses, Laplace domain								
(M_1, M_3)	-20.6	-1.5	30.3	13.3	-4.5	-2.5	-1.4	2.7
(M_1, M_2)	-28.9	-2.2	32.8	20.1	-6.5	-2.0	0.2	3.2
(M_2, M_3)	-45.9	-1.9	35.9	25.1	-5.3	-4.7	-3.9	4.8
all cases	-45.9	-1.9	35.9	20.1	-6.5	-3.1	0.2	3.6
one added mass, time domain								
all cases	-7.2	-5.2	-2.5	5.4	-7.2	-5.2	-2.5	5.4
two added masses, time domain								
(M_1, M_3)	-31.2	-6.4	30.7	17.4	-10.4	-6.0	-2.8	6.5
(M_1, M_2)	-39.5	-1.7	56.7	28.0	-4.1	-2.2	-0.7	2.5
(M_2, M_3)	-64.5	-2.8	96.4	45.3	-8.6	-7.7	-5.4	7.7
all cases	-64.5	-3.6	96.4	32.3	-10.4	-5.3	-0.7	6.0

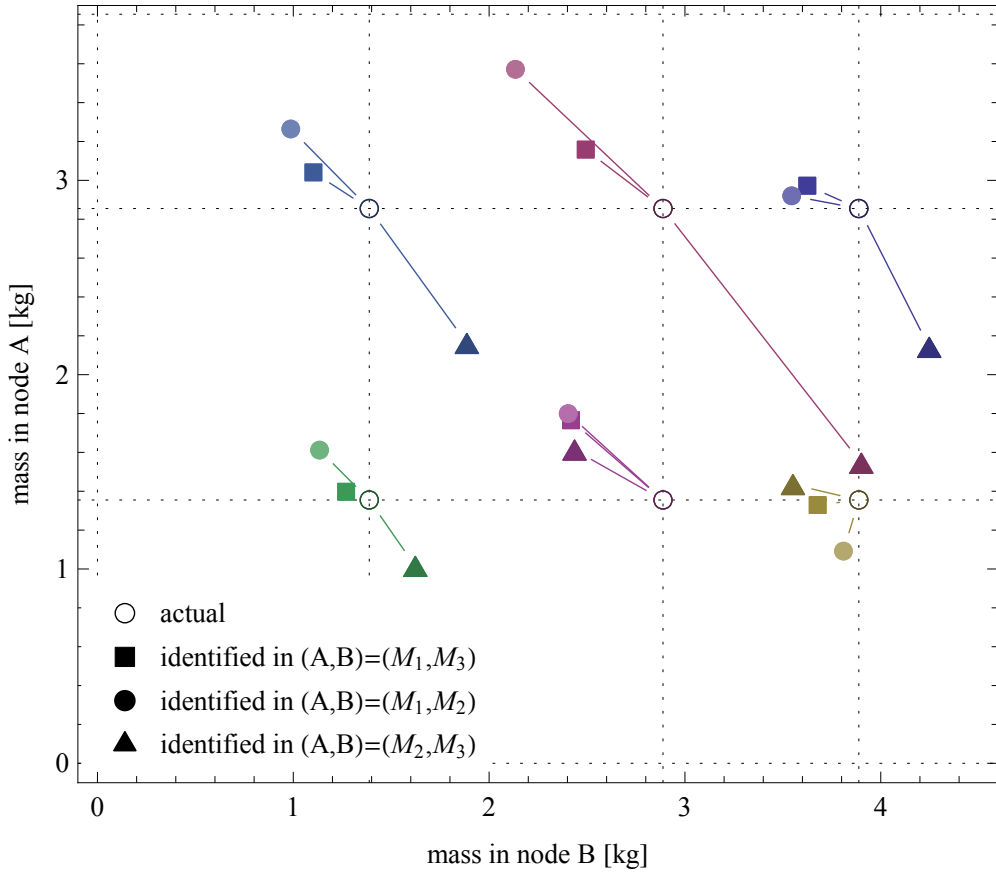


Figure 5: Identification of two added masses in Laplace domain: actual added masses (centers of circles) and identified masses (markers) for the three considered combination of nodes

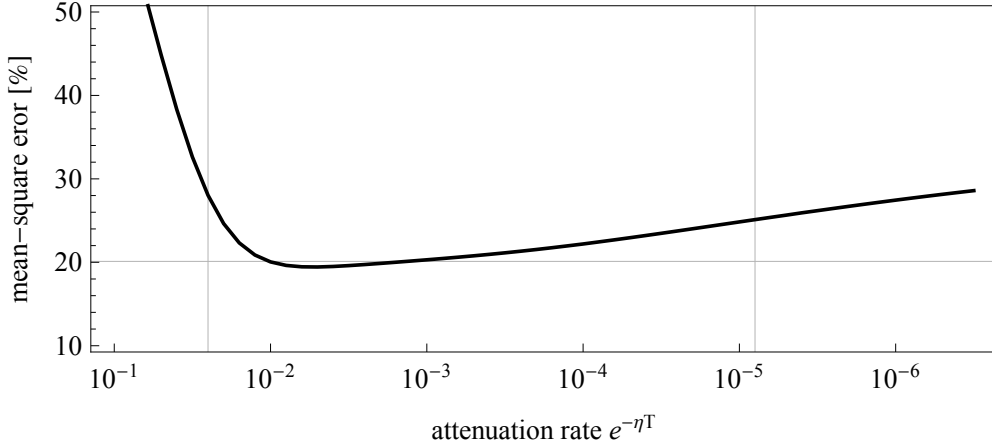


Figure 6: Identification of two added masses in frequency domain: mean-square relative identification error Eq. (33) in dependence on the attenuation rate of the exponential FFT window at the end of the considered time interval. The horizontal gridline mark the 20.1% rms error of identification in Laplace domain, while the vertical gridlines mark the beginning and the end of the reliability set \mathbf{L}_η defined in Eq. (31)

ill-conditioning of the problem: two closely located masses influence structural response in a very similar way, and it is difficult to clearly separate their individual contributions with noisy measurements. The validity of such an explanation is confirmed by a comparison of the relative identification error obtained for masses placed further apart (13.3% for nodes M_1 and M_3) to the much higher errors obtained for masses placed in neighboring nodes (20.1% and 25.1%), and it is especially evident for modification Case No 4, see Fig. 5. These errors still compare favorably to the errors obtained in the time-domain analysis (17.4%, 28.0% and 45.3%, respectively).

The total modification mass (that is the sum of the two simultaneously added masses) can be identified in Laplace domain with a high rms accuracy of 3.6% overall (or even 2.8% for nodes M_1 and M_3), which is at the level comparable to the accuracy obtained for a single unknown mass. Again, such an accuracy is significantly better than the accuracy obtained in time-domain analysis (6.0% overall).

Robustness of the Laplace-domain approach vs. the frequency-domain analysis can be confirmed by comparing the Laplace-domain identification error to the frequency-domain errors, see the horizontal gridline and the curve in Fig. 6. It can be noticed that the Laplace-domain error (represented by the horizontal gridline) is significantly lower than the frequency-domain error (the curve) for most of the domain of reliability, and that it is only negligibly larger than the minimum value of the frequency-domain error. As an additional disadvantage of the frequency-domain approach, it can be noticed that the identification results are not stable in the range of the decay rates commonly used in experimental practice (1% to 4% window attenuation at the end of the time interval): the relative identification error strongly varies between 20% and 40%.

5. Conclusions

This paper proposes a nonparametric, Laplace-domain method for identification of structural modifications, including the first- and second-order sensitivity analysis of the problem. A reduced nonparametric model of the unmodified structure is used, which consists of only a small subset of structural impulse responses. Such a model can be collected in a purely experimental procedure: there is no need for any parametric structural modelling, including the laborious processes of model design and updating. A laboratory 3D truss structure with 70 elements and 26 nodes is used for experimental verification. A total of 30 cases of single and two concurrent modifications of nodal masses are successfully identified using a single impact test excitation and a single test sensor.

In comparison to the time-domain formulation proposed earlier [31], the advantages of the Laplace-domain approach can be summarized as follows:

- Significantly higher accuracy, as assessed in terms of the relative identification errors.
- More difficult identification cases can be reliably addressed (two concurrent mass modifications in neighboring nodes).
- Reduction of the computational cost by two to three orders of magnitude.

The identification time is shorter, because the crucial step of numerical deconvolution is much less time-consuming in Laplace domain than in time domain. Moreover, a large number of frequency lines that are poorly represented in the experimental excitation can be explicitly neglected, which decreases further the computational cost, increases the signal-to-noise ratio and improves the identification. In comparison to the frequency-domain formulation, the proposed Laplace-domain approach averages out the numerical instabilities related to the specific choice of the decay rate.

In specific applications, a disadvantage of the Laplace-domain formulation might be the lack of a direct access to reliable time-histories of structural response. In time-domain formulation, the time-domain responses constitute an inherent part of the identification procedure. In Laplace domain, they need to be reverse-engineered based on their Laplace transforms modeled nonparametrically within their reliability domains, which is a nontrivial operation that usually demands additional processes of optimization and regularization [40]. Moreover, the responses computed in both approaches are numerically regularized in different domains, so that they might not be equivalent: a properly regularized Laplace- or frequency-domain response need not correspond to a properly regularized time-domain response.

6. Acknowledgement

Financial support of the National Science Centre, Poland, granted through the projects “Ad-DAMP” (DEC-2014/15/B/ST8/04363) and “AIA” (DEC-2012/05/B/ST8/02971), is gratefully acknowledged.

References

- [1] T. Stepinski, T. Uhl, W. Staszewski, *Advanced Structural Damage Detection: From Theory to Engineering Applications*, John Wiley & Sons, Ltd, 2013.
- [2] W. Ostachowicz, A. Güemes, *New Trends in Structural Health Monitoring*, Springer, 2013.
- [3] K. Worden, C. Farrar, The fundamental axioms of structural health monitoring, *Philosophical Transactions of the Royal Society A: Mathematical, Physical and Engineering Sciences* 463 (2082) (2007) 1639–1664.
- [4] C. Farrar, K. Worden, An introduction to structural health monitoring, *Philosophical Transactions of the Royal Society A: Mathematical, Physical and Engineering Sciences* 365 (1851) (2007) 303–315.
- [5] H. Wenzel, D. Pichler, *Ambient Vibration Monitoring*, John Wiley & Sons, Ltd, 2005.
- [6] J. Brownjohn, Structural health monitoring of civil infrastructure, *Philosophical Transactions of the Royal Society A: Mathematical, Physical and Engineering Sciences* 365 (1851) (2007) 589–622.
- [7] V. Giurgiutiu, *Structural Health Monitoring of Aerospace Composites*, Academic Press, 2015.
- [8] R. Ghoni, M. Dollah, A. Sulaiman, F.M. Ibrahim, Defect Characterization Based on Eddy Current Technique: Technical Review, *Advances in Mechanical Engineering* 2014 (182496).
- [9] S. Bagavathiappan, B.B. Lahiri, T. Saravanan, J. Philip, T. Jayakumar, Infrared thermography for condition monitoring—A review, *Infrared Physics & Technology* 60 (2013) 35–55.
- [10] W. Ostachowicz, P. Kudela, M. Krawczuk, A. Zak, *Guided Waves in Structures for SHM*, John Wiley & Sons, Ltd, 2012.
- [11] M. Kharrat, M.N. Ichchou, O. Bareille, W. Zhou, Pipeline inspection using a torsional guided-waves inspection system. Part 1: Defect identification, *International Journal of Applied Mechanics* 6 (4) (2014) 1450034.
- [12] C.-P. Fritzen, P. Kraemer, Self-diagnosis of smart structures based on dynamical properties, *Mechanical Systems and Signal Processing* 23 (6) (2009) 1830–1845.
- [13] P. Kolakowski P, L.E. Mujica, J. Vehí, Two Approaches to Structural Damage Identification: Model Updating vs. Soft Computing, *Journal of Intelligent Material Systems and Structures* 17 (2006) 63–79.
- [14] C.-P. Fritzen, *Vibration-Based Techniques for Structural Health Monitoring*, [in:] *Structural Health Monitoring* (eds D. Balageas, C.-P. Fritzen and A. Güemes), ISTE, London, UK, 2006.
- [15] W. Ostachowicz, M. Krawczuk, M. Cartmell, The location of a concentrated mass on rectangular plates from measurements of natural vibrations, *Computers & Structures* 80 (16–17) (2002) 1419–1428.

- [16] A. Garcia-Palencia, E. Santini-Bell, J.D. Sipple, M. Sanayei, Structural model updating of an in-service bridge using dynamic data, *Structural Control and Health Monitoring* 22 (10) (2015) 1265–1281.
- [17] J.E. Mottershead, M.I. Friswell, Model updating in structural dynamics: A survey, *Journal of Sound and Vibration* 167 (2) (1993) 347–375.
- [18] A. Rytter, *Vibrational Based Inspection of Civil Engineering Structures*, PhD thesis, Department of Building Technology and Structural Engineering, Aalborg University, Denmark, 1993.
- [19] S. Casciati, L. Faravelli, Quantity vs. Quality in the Model Order Reduction (MOR) of a linear system, *Smart Structures and Systems* 13 (1) (2014) 99–109.
- [20] A. Deraemaeker, K. Worden, *New Trends in Vibration Based Structural Health Monitoring*, Springer Vienna, 2010.
- [21] S.W. Doebling, C.R. Farrar, M.B. Prime, A summary review of vibration-based damage identification methods, *The Shock and Vibration Digest* 30 (1998) 91–105.
- [22] I. Antoniadou, G. Manson, W.J. Staszewski, T. Barszcz, K. Worden, A timefrequency analysis approach for condition monitoring of a wind turbine gearbox under varying load conditions, *Mechanical Systems and Signal Processing* 64–65 (2015) 188–216.
- [23] K. Dzierżych, W.J. Staszewski, B. Basu, T. Uhl, Wavelet-based detection of abrupt changes in natural frequencies of time-variant systems, *Mechanical Systems and Signal Processing* 64–65 (2015) 347–359.
- [24] M. Rucka, K. Wilde, Neuro-wavelet damage detection technique in beam, plate and shell structures with experimental validation, *Journal of Theoretical and Applied Mechanics* 48 (3) (2010) 579–604.
- [25] C.S. Sakaris, J.S. Sakellariou, S.D. Fassois, A time series generalized functional model based method for vibration-based damage precise localization in structures consisting of 1D, 2D, and 3D elements, *Mechanical Systems and Signal Processing* 74 (2016) 199–213.
- [26] P.B. Dao, W.J. Staszewski, Lamb wave based structural damage detection using cointegration and fractal signal processing, *Mechanical Systems and Signal Processing* 49 (1–2) (2014) 285–301.
- [27] S. Casciati, Response surface models to detect and localize distributed cracks in a complex continuum, *Journal of Engineering Mechanics* 136 (9) (2010) 1131–1142.
- [28] O.R. de Lautour, P. Omenzetter, Damage classification and estimation in experimental structures using time series analysis and pattern recognition, *Mechanical Systems and Signal Processing* 24 (5) (2010) 1556–1569.
- [29] L.E. Mujica Delgado, *A hybrid approach of knowledge-based reasoning for structural assessment*, PhD thesis, University of Girona, 2006.
- [30] K. Mendrok, P. Kurowski, Operational modal filter and its applications, *Archive of Applied Mechanics* 83 (4) (2013) 509–519.
- [31] G. Suwała, L. Jankowski, A model-free method for identification of mass modifications, *Structural Control and Health Monitoring* 19 (2) (2012) 216–30.
- [32] P. Kołakowski, M. Wikło, J. Holnicki-Szulc, The virtual distortion method—a versatile reanalysis tool for structures and systems, *Structural and Multidisciplinary Optimization* 36 (3) (2008) 217–234.
- [33] Q. Zhang, L. Jankowski, Z. Duan, Simultaneous identification of excitation time histories and parametrized structural damages, *Mechanical Systems and Signal Processing* 33 (2012) 56–68.
- [34] M. Mroz, L. Jankowski, J. Holnicki-Szulc, VDM-based identification of localized damage induced damping, *Proceedings of the 5th European Workshop on Structural Health Monitoring (EWSHM)* (2010) 988–993.
- [35] L. Jankowski, Off-line identification of dynamic loads, *Structural and Multidisciplinary Optimization* 37 (6) (2009) 609–623.
- [36] J. Hou, L. Jankowski, J. Ou, Experimental study of the substructure isolation method for local health monitoring, *Structural Control and Health Monitoring* 19 (4) (2012) 491–510.
- [37] P.C. Hansen, *Discrete inverse problems: insight and algorithms*, SIAM, Philadelphia, 2010.
- [38] P. Tazowski, M. Kleiber, Parameter and shape sensitivity of thermo-viscoelastic response, *Computers and Structures* 84 (5–6) (2006) 385–399.
- [39] D.I. Papadimitriou, K.C. Giannakoglou, Aerodynamic shape optimization using first and second order adjoint and direct approaches, *Archives of Computational Methods in Engineering* 15 (4) (2008) 447–488.
- [40] J. Abate, W. Whitt, A unified framework for numerically inverting Laplace transforms, *INFORMS Journal on Computing* 18 (4) (2006) 408–421.